J.Natn.Sci.Foundation Sri Lanka 2019 47 (4): 409 - 420
DOI: http://dx.doi.org/10.4038/jnsfsr.v47i4.9687

RESEARCH ARTICLE

Silver-montmorillonite-conducting polymer composite materials as low-cost oxygen reduction catalysts

K.G.C. Senarathna[1,2*] and R.M.G. Rajapakse[1,3]
[1] *Postgraduate Institute of Science, University of Peradeniya, Peradeniya.*
[2] *Department of Biosystems Technology, Faculty of Technological Studies, Uva Wellassa University of Sri Lanka, Badulla.*
[3] *Department of Chemistry, Faculty of Science, University of Peradeniya, Peradeniya.*

Submitted: 16 March 2018; Revised: 11 October 2018; Accepted: 23 August 2019

Abstract: Throughout the globe, researchers are in quest of electro-catalysts for oxygen reduction reaction (ORR) in order to develop cathode materials for fuel cells (FCs). Although the anodic half-reactions of FCs are fast enough for oxidation of any fuel on cheap catalysts, ORR at the cathode is a slow process even with expensive platinum-based catalysts. Development of low-cost electro-catalysts with reasonably fast kinetics for (ORR) is desirable if fuel cell power is to be utilised in practice. The present study is based on the preparation and characterisation of silver-based electro-catalysts towards ORR. Simple chemical processes were developed to prepare three different electronically conducting nano-composites. Aniline, pyrrole or 3,4-ethyldioxythiophene (EDOT) in between the layer space of silver [Ag (I)] ion exchanged montmorillonite (MMT) undergoes spontaneous polymerisation. During the polymerisation process, Ag(I) cations are reduced to form metallic silver, while aniline, pyrrole or EDOT monomers are converted to polyaniline (PANI), polypyrrole (PPY) and poly (3,4-ethylenedioxythiphene) (PEDOT), respectively. The prepared composites were extensively characterised by X-ray diffraction (XRD), Fourier Transform Infrared (FTIR), X-ray photoelectron spectroscopy (XPS), conductivity measurements, AC-impedance and electrochemical analyses. Electrochemical studies showed that composites are good candidates towards ORR in alkaline electrolyte medium. Ag/MMT/PEDOT showed the best performance in catalytic properties. All three composites showed better performances than that of typical Ag/C composites with a similar mass loading of silver. Although the performances of the cheap composites are somewhat lower when compared to commercially available Pt/C, the performance is sufficient to use the materials as cheap alternatives for FC cathodes.

Keywords: Conducting polymer, electrocatalyst, montmorillonite, oxygen reduction reaction, silver.

INTRODUCTION

The foreknown usable energy crisis is an important problem for the present day scientists to pursue solutions. Fuel cell (FC) is a good alternative energy source that can efficiently generate electricity by consuming fuels and oxygen. FC has fuel flexibility. Hydrogen is the cleanest fuel with highest energy density in terms of mass. Both hydrogen and oxygen can be synthesised by water splitting using photo-catalytic processes and fuels like methanol can be produced from bio-degradable garbage. This means that solutions for the usable energy crisis can be sought from our own surroundings instead of depending on crude oil. However, there are some drawbacks in FC systems. The major problem is the cost of production due to expensive platinum-based catalysts used for both electrodes, particularly, as the cathode for oxygen reduction. Reduction of platinum content is an important step forward in reducing the cost of FCs. Cutting edge research on platinum alloys or platinum-free alloys together with other transition metals are highly active and these catalysts have performed better than naked platinum as revealed by many publications (Wang *et al*., 2012). Moreover, nano-particles of metals or metal alloys have been prepared with supporting materials to increase the surface area and to minimise metal loading (Chung *et al*., 2013; Perini *et al*., 2015).

* Corresponding author (chathuranga@uwu.ac.lk; https://orcid.org/0000-0001-8234-1383)

Abundance of silver on Earth crust is around 0.08 ppm (John, 2001), which is 25 times higher than that of Pt and around 27,300 tonnes had been produced for world market in the year 2015 (George, 2016). Hence, silver is considerably cheaper and more abundant compared to Pt (Holewinski *et al*., 2014). Moreover, silver-carbon black and silver-polypyrrole composites have been synthesised and used as ORR electrocatalysts (Singh & Buttry, 2012; Senarathna *et al*., 2015). MMT is a good catalyst due to its structural arrangement in gas trapping and better binding properties (Senarathna *et al*., 2016). Hence, MMT conducting polymer (CP) composites have been used as catalyst for ORR and there are several publications reporting their activities towards ORR (Rajapakse *et al*., 2010; Senarathna *et al*., 2016).

METHODOLOGY

Chemicals

All chemicals used were purchased from Sigma-Aldrich. Silver nitrate (assay > 99 %, $AgNO_3$), nitric acid 90 %, freshly distilled aniline, pyrrole and EDOT (assay > 97 %, $C_6H_6O_2S$), commercial bentonite clay as MMT source, platinum on carbon support Pt/C (20 % w/w) and Nafion® (5 % w/w in propanol solution) were used in this study.

Purification of bentonite

Bentonite clay was purified by the procedure given below. Twenty grams of bentonite clay was suspended in 500 mL distilled deionised water by shaking for 12 h at room temperature to remove water soluble impurities. The dispersion was centrifuged and the supernatant was discarded. The remaining solid was washed two more times by repeating the same procedure. The solid was then suspended in 1.0 M HNO_3 and the above procedure was repeated three times. The solid mass obtained was then suspended in 6 % H_2O_2 and the procedure was repeated thrice. This has resulted in pure MMT with H^+ Substitutes for cations in interlayer space (Zhao *et al*., 2016; Senarathna & Rajapakse, 2018).

Preparation of Ag(I) ion-exchanged montmorillonite [Ag(I)/MMT]

$AgNO_3$ (1.71 g) was dissolved in 0.10 mol dm^{-3} HNO_3 solution (10.0 mL) in a 100 mL volumetric flask and diluted up to the mark to prepare 0.10 moldm^{-3} Ag^+(aq) solution. Purified MMT (0.50 g) was added to the prepared 0.10 mol dm^{-3} Ag^+ (aq) solution (10 mL) and stirred for 48 h. The suspension obtained was centrifuged and the slurry of Ag(I)/MMT was collected by discarding the supernatant. The solid mass was washed thrice with distilled water, dried under ambient conditions and powdered in an agate mortar and pestle.

Preparation of Ag/MMT/conducting polymer composites

For the preparation of these types of composites, the amount of silver nitrate was selected so that the Ag content is equal to ~20 % w/w of the total mass of the final product. Then, the amount of monomer was selected so as to have 1:1 molar ratio of Ag: monomer.

Preparation of Ag/MMT/PANI and Ag/MMT/PPY composites

Purified MMT (0.30 g) was added to a solution prepared by mixing 0.10 M Ag(I) solution (10.0 mL) and 0.10 M HNO_3 (10.0 mL). Mixture was sonicated for 2 min and stirred for 48 h. A 0.10 M solution of aniline in 0.10 M HNO_3 (10.0 mL) was added and the mixture was again sonicated for 15 min. Then the reaction mixture was stirred again for 24 h and left for three weeks to allow for the polymerisation of aniline to PANI while shaking it once a day to re-disperse the sediments formed. A green coloured Ag/MMT/PANI composite sample was formed in the container. The composite was separated by discarding the supernatant after centrifugation. It was washed with 0.10 M HNO_3 solution first and then with acetone. The sample obtained was allowed to dry under ambient conditions and powdered in an agate mortar and pestle (theoretical silver content ~21.4 % w/w). The same procedure was followed with 0.10 M pyrrole in 0.10 M HNO_3 solution (10.0 mL) instead of aniline for the preparation of Ag/MMT/PPY composite. The composite was black in colour (theoretical silver content ~22.7 % w/w). The same procedure was followed with EDOT (110 mL) in ethanol (20.0 mL) instead of aniline and blue coloured Ag/MMT/PEDOT composite was obtained (theoretical silver content ~ 19.6% w/w).

Synthesis of Ag/C composite of 20 % w/w Ag

To prepare the Ag/C composite, Vulcan XC-72R (0.430 g) was added to a 0.05 mol dm^{-3} Ag^+ (aq) solution (10 mL). Mixture was sonicated for 2 min and then stirred for 48 h. Sodium borohydride (0.11 g) was added and the mixture was again sonicated for 15 min. Then, the reaction mixture was stirred again for 5 h and the black coloured sample formed was separated by discarding the supernatant after centrifugation. It was washed with water and then with acetone. The sample was allowed to dry under ambient conditions and powdered in an agate mortar and pestle (theoretical silver content ~20.0 % w/w).

Characterisation of products

XRD analysis was carried out to identify the crystalline phases of both raw materials and synthesised materials using Siemens D5000 X-ray powder diffractometer (Cu K_α radiation λ = 0.154 nm/scan rate of 1° or 2° per minute /2θ range 3°-80°). Each sample was dried at 150 °C, for 2 h in order to produce its anhydrous form and the XRD analysis was carried out again (2θ range 3°-14°) at 150°C. Particle size, shapes of silver and morphological studies of products were carried out from Hitachi SU6600 Scanning Electron Microscope (SEM) [acceleration voltage =10 kV / Leo 1530 VP Field Emission Gun Scanning Electron Microscope (FE-SEM)]. FT-IR spectra were examined for KBr/ sample pellets (diameter = 13 mm, pressed at a pressure of 5 tonnes, mass ratio of sample : KBr is 1:40). XPS of synthesised materials were characterised using Axis Ultra DLD X-ray Photoelectron Spectrometer and the data were re-plotted and analysed using CasaXPS 2.3 and Origin pro 8.0 software. Powdered samples were pressed at a pressure of 7 tonnes to prepare pellets (surface area of 0.143 cm^2 /thickness was varied) to study the DC conductivity. Prepared pellet was sandwiched between two stainless steel rods and voltage of 0.1 V was applied to the two terminals and the current passed through the pellet was measured and conductivity was calculated using Ohms law. The four-probe techniques proposed by van der Pauw *et al.* was also used (Yao *et al*., 2012). To carry out the electrochemical studies, catalytic ink was prepared by separately dispersing Ag/PANI/MMT, Ag/PPY/MMT or Ag/PEDOT/MMT samples (10 mg each) in a solution formed by mixing ethanol (2.0 mL) and Nafion solution (10 mL). Then the mixture was sonicated for 10 min. The ink (10 mL) thus obtained was deposited on a cleaned and polished glassy carbon (GC) electrode of 0.384 cm^2 active surface area (Jia, 2014). This electrode was dried and used as the working electrode to run cyclic voltammogrammes (CVs) using Metrohm Potentiostat 101 and NOVA 1.7 software. The above procedure was repeated for the preparation of platinum carbon (Pt/C) electrode and silver carbon (Ag/C) electrode using commercially available Pt/C (20% w/w) and prepared Ag/C, respectively. Potentials were applied with respect to the saturated calomel electrode (SCE) and a Pt rod was used as the counter electrode. Scan rate used was 50 mV s^{-1} and 0.10 M KOH (aq) was used as the electrolyte solution. CVs were recorded in N_2-purged and O_2-saturated solutions. Then the electrodes prepared were used as the working electrodes to run a LSV at rotating speeds from 1600 rpm and 5 mV s^{-1} scan rate in oxygen saturated 0.10 M KOH (aq) electrolyte solutions. Polarizing curves were drawn using Nova 1.7 software. All graphs are re-plotted using Origin 8.0 Pro software (Fadley, 2010).

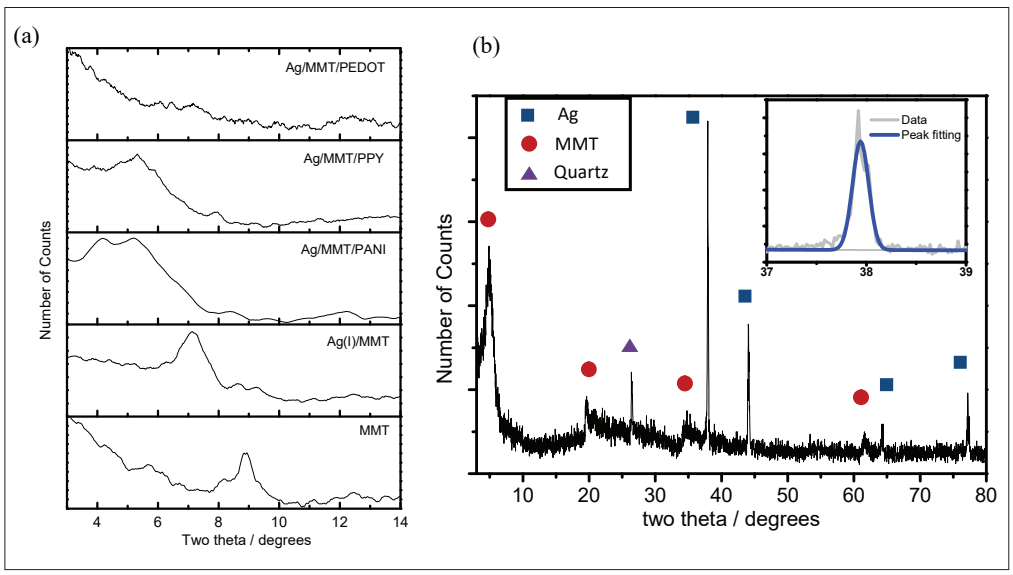

Figure 1: (a) XRD patterns of pure MMT, Ag(I)/MMT and Ag/MMT/conducting polymer composites recorded at 150 °C in the 2θ range from 3° to 14°; (b) XRD spectrum of Ag/MMT/PPY composite at RT from 3° to 80° of 2θ range and the inset is the fitting curve for peak at 38°

RESULTS AND DISCUSSION

XRD analysis

Figure 1(a) shows the XRD patterns of purified MMT, Ag(I)/MMT, Ag/MMT/PANI, Ag/MMT/PPY and Ag/MMT/PEDOT at 150 °C in the range of two theta values corresponding to the diffractions from the (001) basal planes of MMT. The d-values of major peaks obtained at RT and at 150 °C are tabulated on Table 1. According to the data, when purified MMT is heated at 150 °C, for 2 hours, all of the hydrated water molecules are removed and the presence of bare H_3O^+ cations within the interlayer spacing gives a d value of 9.7 Å, whereas MMT at RT shows a d-spacing of 15.0 Å. Since the thickness of a water monolayer around an ion is ~3 Å, it is evident that there are two water layers around H_3O^+ ions present within the interlayer spacing. When H^+ is exchanged for Ag^+, d-spacing change but the change can only be determined if hydration spheres are removed. Therefore, the values of the d-spacing of samples heat-treated at 150 °C correlate directly to the sizes of bare species in the absence of hydration spheres. As such, the replacement of H^+ ions by Ag^+ ions are manifested by the increase in the d-spacing by 2.7 Å. Introducing of PPY and PANI to the interlayer spaces of MMT has further increased the d-spacing by 4.2 Å and 4.6 Å, respectively.

Table 1: Calculated interlayer space distances of different materials at room temperature as well as for the same samples at 150 ˚C

Material	d values / Å	
	at RT	at 150 °C
MMT	15.0	9.7
Ag(I)/MMT	15.6	12.4
Ag/MMT/PANI	17.7	17.0
Ag/MMT/PPY	16.6	16.6
Ag/MMT/PEDOT	No peaks for (001)	

It is interesting to note that the d-spacing of Ag/ MMT/ PANI and Ag/MMT/PPY have not changed considerably due to heat treatment. This is because while Ag atoms do not get hydrated, the formation of conducting polymers also results in the expelling of water from the interlayer spaces. These observations indicate that there are not many water molecules bonded to the MMT sheets in the Ag/MMT/Conducting Polymer composites even at room temperature. Thus, the XRD data provides indirect evidence to the exchange of H^+ by Ag^+ and also the formation of polymers in the interlayer spaces when monomers are introduced. This so happens due to the oxidative polymerisation of pyrrole or aniline by Ag^+ cations thus forming Ag(0) as shown in equations 1, 2 and 3. The presence of Ag(0) in Ag/MMT/PPY is verified by its XRD spectrum recorded in the full range of 2θ values from 0° to 80° which is shown in Figure 1(b). The corresponding diffraction peaks appearing at 2θ values of 5.32°, 19.9°, 35.0° and 62.5° are assigned to diffraction pattern of MMT (circle marks) according to the JCPDS card number 82-1873 while those appearing at 2θ values of 38.0°, 44.3°, 64.5° and 77.0° are assigned to be due to reflections from basal planes of (111), (200), (220) and (311) respectively of Ag metal (square marks) as JCPDS card Number 04-0783. This confirms the presence of both MMT and Ag(0) in the Ag/PPY/MMT composite. Inset of Figure 1(b) is the fitting curve of the peak at 38.0°. Half peak width and the positions are calculated using Origin Pro 8.0 software. Mean crystalline size of silver calculated from Scherer formula is 54.13 nm. XRD pattern of Ag/MMT/PEDOT composite, shown in Figure 1(a) does not show a peak corresponding to (001) plane of MMT. This is due to the exfoliation of MMT layers during the synthesis of Ag/MMT/PEDOT composite.

XPS analysis

High resolution XPS spectra of Ag 3d range for Ag(I)/ MMT, Ag/MMT/PANI and Ag/MMT/PPY compounds are depicted in Figure 2(a). In both Ag/MMT/PANI and Ag/MMT/PPY materials, Ag(I) ions were used to initiate the polymerisation process. Hence, PANI and Ag particles generate simultaneously during the reaction process. Binding energies of Ag $3d_{5/2}$ and $3d_{3/2}$ are 366.9 eV and 373.0 eV, respectively, for Ag(I)/MMT and theoretical values of Ag $3d_{5/2}$ appears around ~368 eV. (Sivanesan *et al*., 2014) This deviation of binding energy is due to the Ag(I) being bonded to the MMT layers. In Ag/MMT/ PANI, binding energies of Ag $3d_{5/2}$ and $3d_{3/2}$ are shifted to 367.5 eV and 374.5 eV, respectively. These values are also different from those of naked silver metal, which appear at 368.2 eV and 374.2 eV, respectively. This may be due to the formation of dative bonds from N atoms of amine units of PANI with silver particles or ions in MMT layers. For Ag/MMT/PPY, both binding energies of Ag $3d_{5/2}$ and $3d_{3/2}$ are shifted to 368.2 eV and 374.2 eV, respectively, (Wei *et al*. 2010) as depicted in Figure 2(b). These values correspond to those of the silver metal, confirming the presence of Ag metal in the composite.

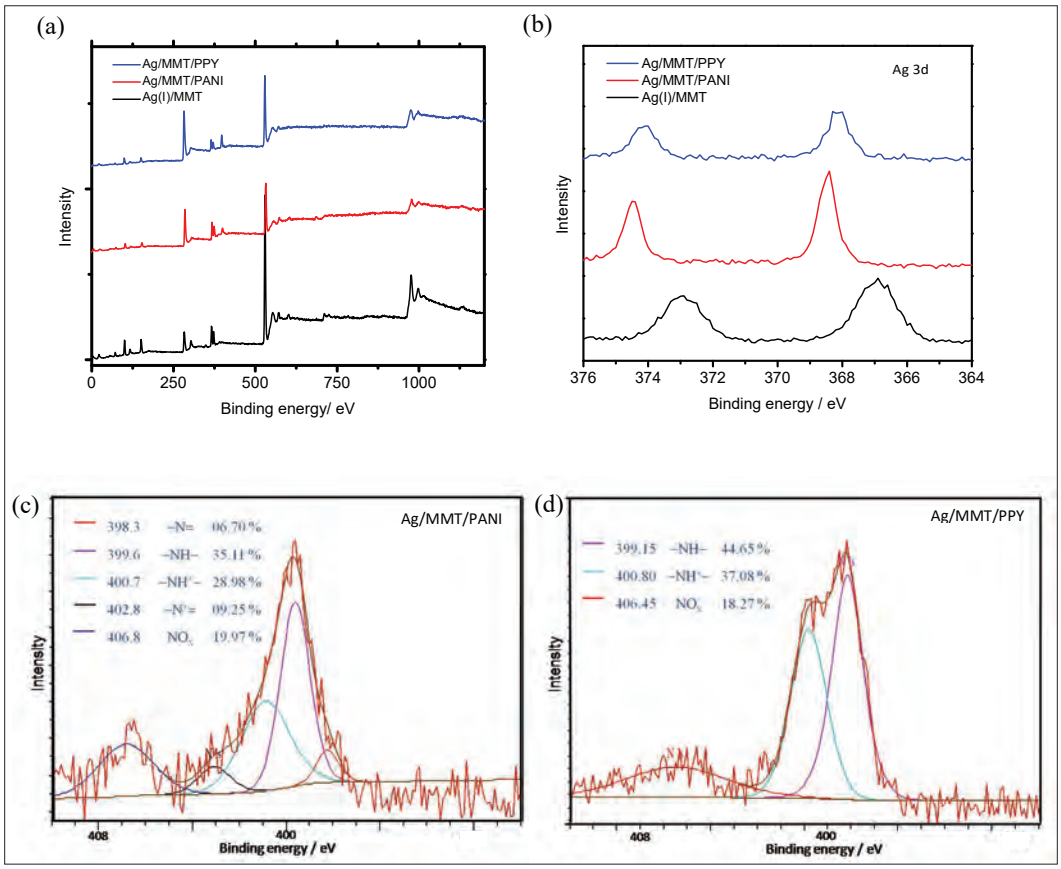

Figure 2: (a) XPS spectra for Ag(I)/MMT, Ag/MMT/PANI and Ag/MMT/PPY; (b) high resolution XPS spectra of Ag 3d; high resolution XPS spectra of N (c) Ag/MMT/PANI and (d) Ag/MMT/PPY

Figure 2(c) shows the XPS N 1s core-level spectra of Ag/MMT/PANI nanocomposite and it consists of five peak components of binding energies (BEs). Bands at BEs of 399.6 eV and 400.7 eV are attributed to the –NH– and $–NH_2^+–$ species and components at 398.3 eV and 402.8 eV are due to the uncharged deprotonated imine (=N–) nitrogen and charged imine ($=NH^+–$) groups of PANI. Hence, the ratio of protonated N atoms to deprotonated N atoms is 1: 1.2. According to the XPS data, =N– to –NH– ratio of Ag/MMT/PANI is 1:4 and this result indicates the presence of ES form of PANI.

Component at around 406.8 eV is usually due to the oxidised N atoms. The possible oxidised N species in this composite is NO_3^- ions. However, no other anions exist in the composite and percentage value of N of NO_3^- ions is half of that of total protonated atoms, hence other protonated N atoms exist in the bonded form with the negatively charged MMT layers. Figure 2(d) shows the XPS N 1s core-level spectra of Ag/MMT/PPY nanocomposite and it consists of three peak components as typical of PPY. BEs at 399.15 eV and 400.80 eV are attributed to the –NH– and $–NH^+–$ species (Menon *et al*., 1996). Hence, ratio of the areas of these nitrogen peaks (1.2:1.0) correlates with the doped state of the PPY (Bala *et al*., 2000). Component at around 406.45 eV is usually due to the oxidised N species and hence this composite also contains NO_3^- ions. Percentage values of N of NO_3^- ions is half of that of protonated N atoms hence other protonated atoms exist in the bonded form with the negatively charged MMT layers.

According to the above characterisations, possible reactions can be suggested for the polymerisation process. Ag(I) initiates the polymerisation of aniline according to the reaction given below. Hence, the metallic silver particles are formed due to the reduction of Ag(I) as shown in equation 1.

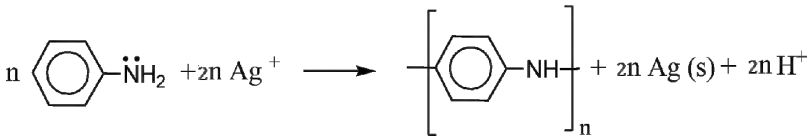

...(1)

Further oxidation of PANI into its Emeraldine and Pernigraniline forms takes place with the amount of oxidant. Ag(I) can induce similar reactions with pyrrole and EDOT as shown in following chemical equations 2 and 3.

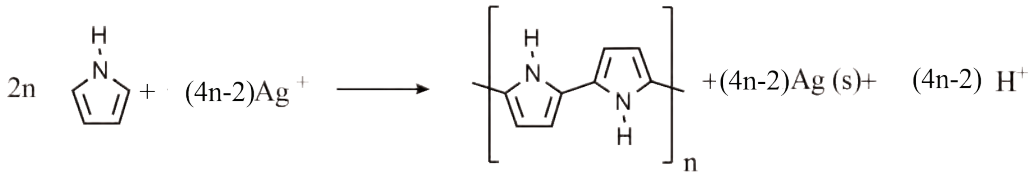

...(2)

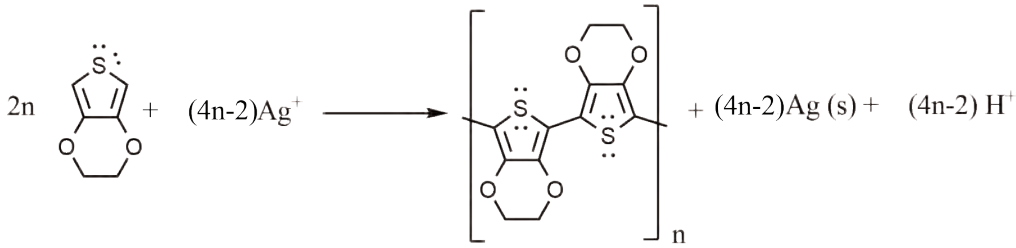

...(3)

FTIR analysis

FTIR spectra of the samples are depicted in Figure 3. All samples have a band at the 1030 cm^{-1}, which is assigned to the Si-O stretching of MMT sheets. Hence, other bands are compared with respect to this band. The Si-O-Si and Si-O-Al deformation vibrations, respectively, appear at 523 cm^{-1} and 466 cm^{-1} and are deformed and shifted due to the effect of exchanged cations (Sogandares & Fry, 1997). All composites show H-O-H bending mode at 1640 cm^{-1} (Cursino *et al*., 2011). However, Ag/MMT/PANI, Ag/MMT/PPY and Ag/MMT/PEDOT show weaker absorptions at 1640 cm^{-1} than that of pure MMT. This is because the polymerisation process leads to removal of water inside the MMT layers as proven by the XRD data. Hence, they are water-repellant materials when compared to pure MMT. Corresponding bands for PANI appears in the Ag/MMT/PANI composites also. However, some bands assigned to PANI are masked by the higher absorbance of characteristic MMT bands. Similarly, Ag/MMT/PPY and Ag/MMT/PEDOT show characteristic bands of PPY and PEDOT, respectively.

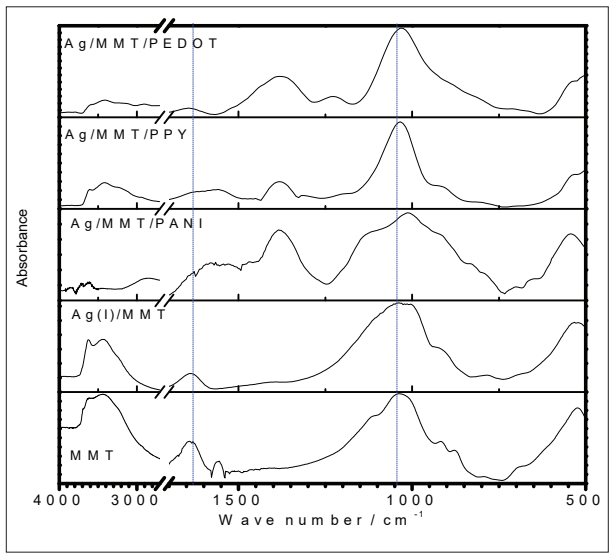

Figure 3: FTIR spectra of Ag(I)/MMT, Ag/MMT/PANI, Ag/MMT/PPY, Ag/MMT/PEDOT and pure MMT, at the range of 4000 cm^{-1} to 2700 cm^{-1} and 1700 cm^{-1} to 500 cm^{-1}

The band at 1400 cm^{-1} appearing in Ag/MMT/PANI, Ag/MMT/PPY and Ag/MMT/PEDOT is assigned to nitrate ions (originating from nitric acid or silver nitrate) within doped polymers (Blinova *et al*., 2009).

SEM images of Ag/MMT/PPY

SEM images of Ag/MMT/PPY composite are shown in Figure 4. Images reveal that the MMT particles are covered by PPY. MMT stacked structures are not clearly seen in the images due to the coverage by polymers. Every image has bright spots around 10 to 200 nm scale. This may be due to the conducting Ag particles or spherical Ag clusters attached with the polymers. The particle sizes match with the data from XRD. Circled area of the image in Figure 4(c) shows a hexagonal silver particle of 160 nm diagonal length. Although the Ag(I) ions are intercalated into the MMT layers, it appears that the Ag metal particles are present outside of MMT. When the pyrrole is introduced to the suspension of Ag(I)/MMT, Ag(I) ions can exist both outside and inside of the MMT layers and the sonication process would lead to the exfoliation of the MMT layers. Ag(I) attached MMT planes are then combined with pyrrole molecules and pyrrole is polymerised while Ag(I) is reduced to Ag particles.

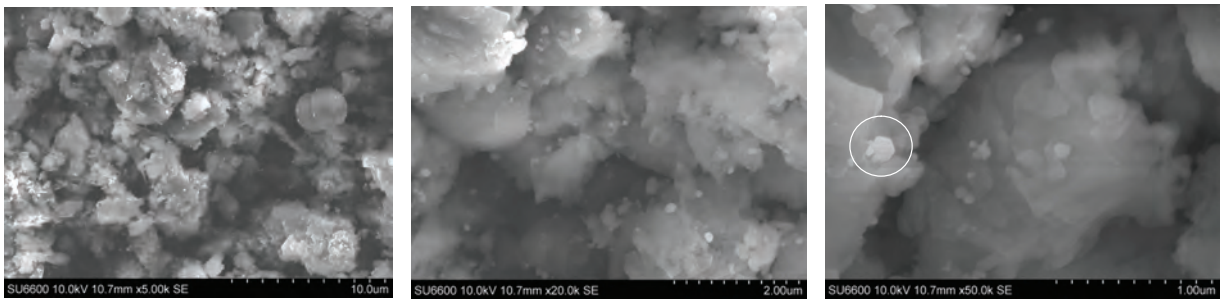

(a) (b) (c)

Figure 4: SEM images of Ag/MMT/PPY

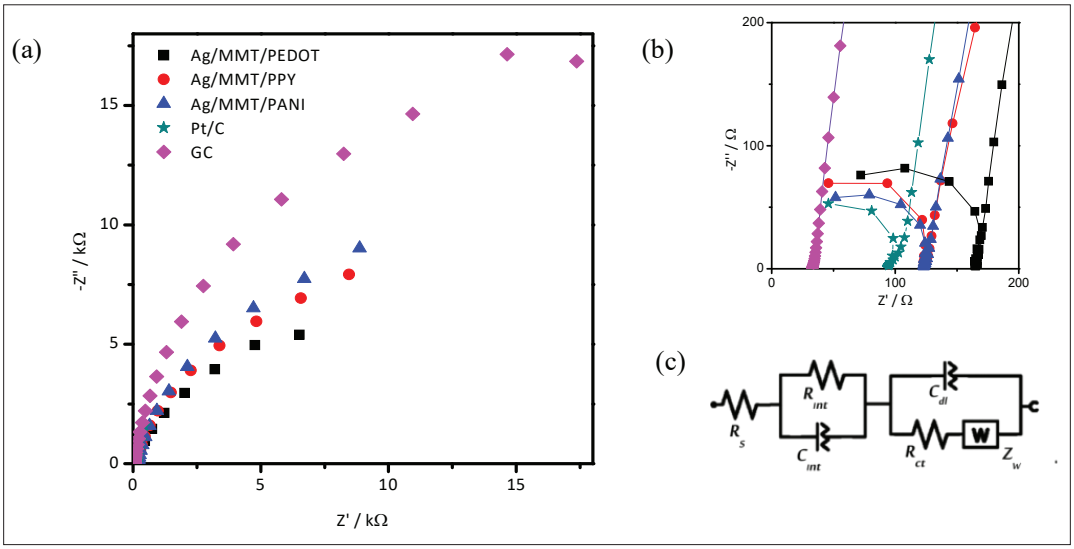

Figure 5: (a) Nyquist plots of EIS for silver-based composite deposited on glass carbon electrodes in 0.10 M KOH solution at their open circuit potentials; (b) high frequency range of Nyquist plots and (c) its corresponding equivalent circuit

DC conductivity studies of composites

The DC conductivity of Ag(I)/MMT is 1.03×10^{-4} S m^{-1} and it is higher than that of pristine MMT (1.24×10^{-6} S m^{-1}) due to the ionic conductivity caused by mobile silver ions. Ag/MMT/PANI, Ag/MMT/PPY and Ag/MMT/PEDOT show conductivities of 5.02, 2.36 and 2.86 S m^{-1}, respectively. This increment of conductivity is due to the presence of conducting polymers and silver nano particles in the composite. Ag/MMT/PANI has the highest conductivity.

AC impedance analysis

EIS spectra for catalyst-deposited GC electrodes in 0.10 M KOH electrolyte are depicted in Figure 5(a) and Figure 5(c) is the modified Randles equivalent circuit suggested for the Nyquist plots obtained.

Catalyst loading was 0.18 mg cm^{-2} for all electrodes. In the circuit R_s, R_{int} and R_{ct}, denote the bulk solution resistance, interfacial resistance and charge-transfer resistance, respectively. C_{int} and C_{dl}, respectively, represent the inter-facial capacitance and the double layer capacitance. Z_w is Warburg impedance. The Nyquist plots at higher frequency ranges are zoomed and displayed in the Figure 5(b). Nova 1.10 software was used for curve fitting and calculating component values. Calculated values for important circuit components are summarised in Table 2. R_{int} depends on the conductivity of the materials hence lowest R_{int} is displayed for Ag/MMT/PANI. However, Ag/MMT/PEDOT shows the lowest R_{ct}. Ideal catalysts should have low R_{ct} and low R_{int}. Hence, all these composites have good catalytic activities. When comparing the values of C_{dl}, Y^0 values of composites are larger than those of Pt/C and GC and N values are smaller than "1". It indicates the deviations from the ideal capacitance nature and is due to the roughness of the surfaces.

Table 2: R_{int}, R_{ct}, C_{dl} data calculated from the EIS spectra

Compound	R_{int}/Ω	R_{ct}/kΩ	C_{dl}	
			Y^0 / μS^{-N}	N
Glassy carbon (GC)	-	29.0	14.0	0.98
Pt/C	84.6	12.0	1.46	0.85
Ag/MMT/PANI	89.1	14.2	74.1	0.89
Ag/MMT/PPY	103.4	11.7	60.6	0.92
Ag/MMT/PEDOT	104.5	9.1	63.9	0.91

Cyclic voltammetric studies

ORR kinetics is faster in alkaline electrolytes than in acid electrolytes and Pt, Ag or some other metals help hydroxide ions to decompose rapidly, and able to increase the potential close to the theoretical potentials of the oxygen electrode (Singh & Buttry, 2012). Moreover, Ag particles are not much stable in the acidic medium, but they are stable catalysts towards ORR in alkaline medium (Liu & Chen, 2013). Hence, in this study, the characteristics of oxygen reduction at silver-based catalyst electrodes are studied in alkaline media.

Figure 6(a) depicts the CV of Ag/MMT/PANI in nitrogen-saturated 0.10 M KOH solution at a potential scan rate of 50 mV s^{-1}. It is shown in the potential window of -1.0V to + 1.0 V. In the CV, four anodic current peaks are clearly observed at +0.31 V, +0.41 V, +0.74 V and +0.80 V as indicated by A1 to A4, respectively. The small peak A1 could be attributed to the formation of a monolayer of AgOH by oxidizing Ag(0) to Ag(I) species and the peak A2 is attributed to the formation of inner hydrous oxide layers (Liu & Chen, 2013). More compact outer oxide layers and Ag_2O form at A3 and A4 anodic peaks which are characteristic to silver electrodes. A5 is for the water oxidation (oxidation of OH^- to O_2). In the reverse scan, 3 cathodic peaks appear at +0.40 V, +0.05 V and -0.40 V which are labelled as C1 to C3, respectively. C1 and C2 are attributed to the reduction of the silver oxides formed during the anodic potential scan to form AgOH and Ag(0), respectively. Such characteristic CV featured from silver indicate that the surface clean Ag nano-particles that are supported on MMT/polymer matrix exhibit high electrochemical activity. C3 is for the reduction of oxygen formed at A5.

CV for Ag(I)/MMT is depicted in Figure 6(b). CV shows all characteristic peaks corresponding to silver due to the presence of Ag(I). Higher current gains than that of Ag/MMT/PANI are observed for all characteristic peaks which may be due to higher amount of silver content present in Ag/MMT/PANI. However, the peaks are shifted to positive values in anodic sweep and shifted to negative potentials in cathodic sweep of the CV and ORR peak is very low when compared to that of Ag/MMT/PANI. The stability of Ag/MMT/PANI has also been evaluated by CV measurements.

According to Figure 6(c), there is only around 20 % change of the current density of CV profile even after 1000 cycles. This indicates the considerable electrochemical stability of the Ag/MMT/PANI catalyst. Considering the

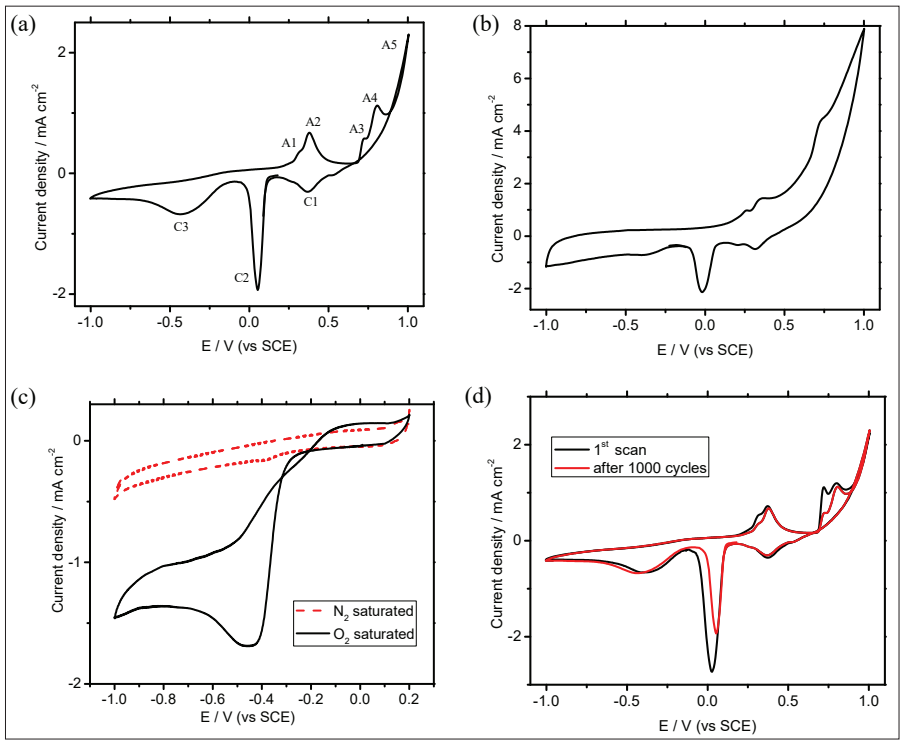

Figure 6: CV of (a) Ag/MMT/PANI and (b) Ag(I)/MMT at nitrogen-saturated 0.10 M KOH solution. CVs of (c) Ag/MMT/PANI in N_2 and O_2 saturated systems between potential range -1.0 V to +0.20 V and (d) Ag/MMT/PANI compared with 1st cycle and after 1000 cycles

ORR catalytic features, Figure 6(d) shows the CVs for Ag/MMT/PANI in N_2-saturated and O_2-staurated 0.10 M KOH solution between +0.20 V and −1.0 V at 50 mV s^{-1} scan rate. The CV of the N_2-purged system is featureless. This means that the reduction peaks observed are not due to reduction of the conducting polymer. This is clearly understandable because PPY, PANI and PEDOT are converted to their reduced forms well before –0.40 V. However, when the electrolyte is saturated with oxygen gas, the oxygen reduction is clearly observed in the negative potential range after –0.40 V with respect to the saturated calomel electrode. The cathodic wave with a peak potential at around −0.42 V is attributed to O_2 reduction. As such, our Ag/MMT/PANI catalyst acts as a good catalyst for the ORR that is very much suitable to be utilised in fuel cells. The procedure was repeated in order to confirm the catalytic property and shows the same performance.

Figure 7(a) depicts the CV of Ag/ MMT/PPY in nitrogen-saturated 0.10 M KOH solution between potentials +1.0 V and −1.0 V at 50 mV s^{-1} scan rate. CV is similar to that of Ag/MMT/PANI. However, the peak assigned to formation of monolayer of AgOH is diminished and only 3 anodic current peaks are clearly observed at +0.35 V, +0.74 V and above +0.80 V, which are labelled as A1, A2 and A3, respectively. A1 and A2 could be attributed to the formation of AgOH and Ag_2O, respectively, and A3 is for the water oxidation to form O_2. In the reverse scan, usual cathodic peaks appeared at +0.40 V, +0.00 V and -0.45 V, which are labelled as C1, C2 and C3, respectively. C1 and C2 are attributed to the reduction of the silver oxide back to AgOH and Ag(0), respectively, and C3 is for the ORR.

Considering the ORR catalytic features, Figure 7(b) shows the CVs for an Ag/MMT/PPY in N_2-saturated and O_2 – saturated 0.10 M KOH between potentials +0.2 V and −1.0 V at 50 mV s^{-1} scan rate. Compared to the featureless CV in the N_2 – saturated electrolyte, a large reduction current peak around −0.42 V is seen in the O_2 – saturated conditions, indicating the electrocatalytic activity of the composite for the ORR. Peak current density is considerably higher than that of Ag/MMT/PANI and shifted to the positive direction.

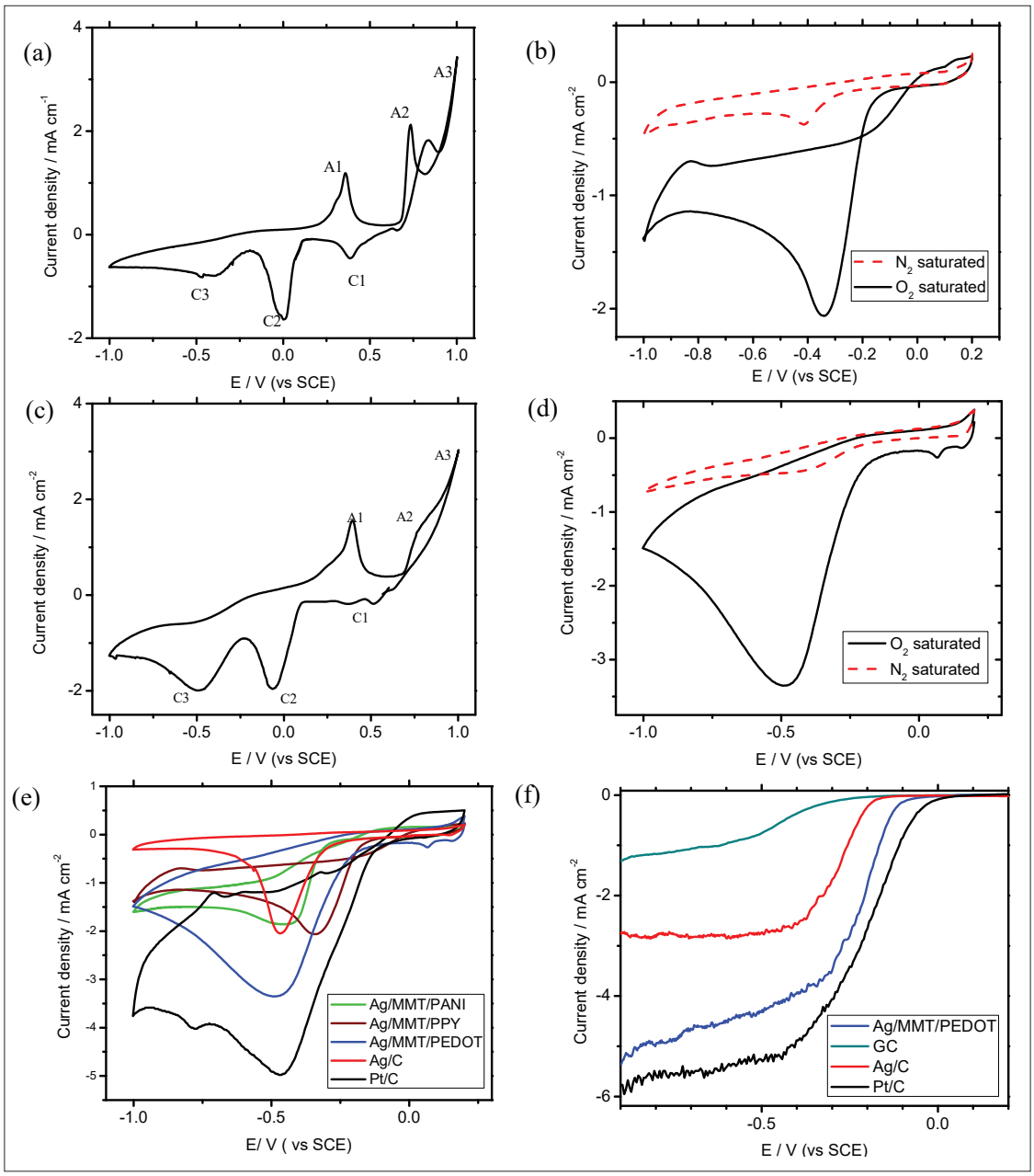

Figure 7: (a) CV of Ag/MMT/PPY and (c) Ag/MMT/PEDOT at N_2 saturated 0.10 M KOH solution between potential range -1.0 V to +1.0 V; (b) CVs of Ag/MMT/PPY and (d) Ag/MMT/PEDOT in N_2 and O_2 saturated systems between potential -1.0 V to +0.20 V with respect to SCE; (e) CVs of Ag/MMT/PANI, Ag/MMT/PPY, Ag/MMT/PEDOT, Ag/C and Pt/C together and (f) RDE data of Ag/MMT/PEDOT, Ag/C, Pt/C and bare GC electrodes.

Figure 7(c) depicts the CV of Ag/ MMT/PEDOT in nitrogen-saturated 0.10 M KOH solution between potentials +1.0 V and −1.0 V at 50 mV s^{-1} scan rate. This CV also shows the characteristic peaks shown by Ag/ MMT/PANI and Ag/ MMT/PPY. Anodic and cathodic current peaks are labeled same as Ag/ MMT/PPY. However, the peaks are broader than that of Ag/ MMT/PPY and A1 and A2 are shifted to +0.42 V and +0.75 V, respectively and A3 peak for the water oxidation is also observed in the CV. In the cathodic sweep of the CV, usual C1, C2 and C3 cathodic peaks appeared at +0.40 V, −0.08 V and –0.50 V, respectively.

Figure 7(d) shows the CVs of the Ag/MMT/PEDOT electrode in 0.10 M KOH saturated with N_2 or O_2 in the potential range from -1.0 V to +0.2 V at scan rate of 50 mV s^{-1}. Compared to the CV in the N_2-saturated electrolyte, a large reduction current peak around −0.32 V from ORR can be seen in the O_2-saturated electrolyte, indicating the high electrocatalytic activity of the composite for the ORR. Peak current density is considerably higher than that of Ag/MMT/PANI and Ag/MMT/PPY and peak potential is shifted to positive potentials showing lower over-potentials for ORR. In order to compare the catalysts with standard electrodes for their activities towards ORR, we have repeated the experiments with O_2-saturated KOH solutions with just the bare glassy carbon electrode, Ag/C (20% Ag w/w) and Pt/C (20% Pt w/w) as the working electrodes and keeping all the other parameters essentially the same as those used in CV experiments done with Ag/MMT/PANI, Ag/MMT/PPY and Ag/MMT/PEDOT working electrodes. Figure 7(e) shows the CVs of all synthesised silver-based composites together with Ag/C and Pt/C in O_2 saturated 0.10 M KOH solution between potential range -1.0 V to +0.2 V. Ag/MMT/PPY and Ag/MMT/PEDOT composites show the positive shift of the onset potential values. Cathodic peak current density values of Ag/C, Ag/MMT/PANI, Ag/MMT/PPY, Ag/MMT/PEDOT and Pt/C are 1.8, 1.7, 1.9, 3.0 and 4.5 mA cm^{-2} and these data reveal that our composites have better performance than that of Ag/C composites with the same silver loading. However, the novel catalysts show lower ORR activities than that of commercially available Pt/C.

I-V polarization curves

ORR performance is further studied with the linear sweep voltammetry (LSV) measurements on a rotating disk electrode (RDE) of Ag/MMT/PEDOT electrode along with the naked GC, Ag/C (20% Ag w/w) and Pt/C (20% Pt w/w) electrodes. LSV is run under O_2 saturated condition in 0.10 M KOH solutions at a scan rate of 5mV s^{-1} and a rotation rate of 1600 rpm within the range of + 0.5 V to -1.0 V. As shown in Figure 7(f), the onset potentials for oxygen reduction at the Pt/C, Ag/MMT/ PEDOT, Ag/C and GC are +0.05 V, -0.05 V, -0.15 V and -0.24 V, respectively. The limiting diffusion current densities at -0.20 V for the Pt/C, Ag/MMT/PEDOT, Ag/C and GC electrodes are 2.43, 1.71, 0.02 and 0.00 mA cm^{-2}, respectively. At -0.6 V, current values have been changed to 5.5, 4.6, 2.8 and 1.0 mA cm^{-2}, respectively. These results are consistent with the CV data and confirm the significant contributions to the ORR electro-catalytic activity of Ag/MMT/PEDOT.

CONCLUSIONS

The Ag/MMT/PANI, Ag/MMT/PPY and Ag/MMT/PEDOT composites were prepared and their morphological and chemical behaviours as well as conducting properties were characterised. XPS and XRD data confirm that the Ag(I) ions participate in the polymerisation and are reduced to Ag(0). The Ag/MMT/PANI composite contains Ag nanoparticles and emeraldine salt form of PANI intercalated within the interlayer space of MMT. Ag/MMT/PPY composite also shows the similar morphological structure. However, MMT layers are partially exfoliated and Ag particles around 10 nm to 200 nm diameter sizes are bonded with the PPY outside the MMT layers. In the Ag/MMT/PEDOT composites, MMT layers are totally exfoliated in the successfully polymerised PEDOT matrix. All composites show high conductivity and the highest is 5.02 S m^{-1} for Ag/MMT/PANI which is the highest recorded value for clay / electronically conducting polymer composites. Electrochemical analysis shows that all composites have good catalytic activity towards ORR and have enhanced properties Ag/C. Ag/MMT/PEDOT shows the highest performance among these three composites and it has competitive performance with commercially available Pt/C. Therefore, all three composites are suitable for application as low-cost fuel cell cathodes; Ag/MMT/PEDOT being the best.

Acknowledgements

Authors gratefully acknowledge the financial assistance by the Higher Education for Twenty First Century (HETC) Grant.

REFERENCES

Bala P., Samantaray B.K. & Srivastava S.K. (2000). Dehydration transformation in Ca-montmorillonite. *Bulletin of Materials Science* **23**(1): 61–67. DOI: https://doi.org/10.1007/BF02708614

Blinova N.V., Stejskal J., Trchová M., Sapurina I. & Ćirić-Marjanović G. (2009). The oxidation of aniline with silver nitrate to polyaniline-silver composites. *Polymer (Guildf)* **50**(1): 50–56. DOI: https://doi.org/10.1016/j.polymer.2008.10.040

Chung H.T., Won J.H. & Zelenay P. (2013). Active and stable carbon nanotube/nanoparticle composite electrocatalyst for oxygen reduction. *Nature Communications* **4**(1): 1922. DOI: https://doi.org/10.1038/ncomms2944

Cursino A.C.T., Mangrich S., Eduardo F., Mangrich A.S. & Da Costa Gardolinski J.E.F. (2011). Effect of confinement

of anionic organic ultraviolet ray absorbers into two-dimensional zinc hydroxide nitrate galleries. *Journal of the Brazilian Chemical Society* **22**(6): 1183–1191. DOI: https://doi.org/10.1590/S0103-50532011000600026

Fadley C.S. (2010). X-ray photoelectron spectroscopy: Progress and perspectives. *Journal of Electron Spectroscopy and Related Phenomena* **178–179**(C): 2–32. DOI: https://doi.org/10.1016/j.elspec.2010.01.006

George M.W. (2016). *Silver, Mineral Commodity Summaries*. U.S. Geological Survey, USA.

Holewinski A., Idrobo J.C. & Linic S. (2014). High-performance Ag-Co alloy catalysts for electrochemical oxygen reduction. *Nature Chemistry* **6**(9): 828–834. DOI: https://doi.org/10.1038/nchem.2032

Jia Z. (2014). Rotating electrode methods and oxygen reduction electrocatalysts. In: *Rotating Electrode Methods and Oxygen Reduction Electrocatalysts*, pp. 199–229. Elesevier. DOI: https://doi.org/10.1016/B978-0-444-63278-4.00006-9

John E. (2001). *An A-Z Guide to The Elements*, pp. 539. Oxford University Press, UK. DOI: https://doi.org/978-0-19-960563-7

Liu M. & Chen W. (2013). Green synthesis of silver nanoclusters supported on carbon nanodots: enhanced photoluminescence and high catalytic activity for oxygen reduction reaction. *Nanoscale* **5**(24): 12558–12564. DOI: https://doi.org/10.1039/c3nr04054b

Menon V.P., Lei J. & Martin C.R. (1996). Investigation of molecular and supermolecular structure in template-synthesized polypyrrole tubules and fibrils. *Chemistry of Materials* **8**(8): 2382–2390. DOI: https://doi.org/10.1021/cm960203f

Perini L., Durante C., Favaro M., Perazzolo V. & Agnoli S. (2015). Metal-support interaction in platinum and palladium nanoparticles loaded on nitrogen-doped mesoporous carbon for oxygen reduction reaction. *ACS applied material and Interfaces* **7**(2): 1170–1179. DOI: https://doi.org/10.1021/am506916y

Rajapakse R.M.G., Murakami K., Bandara H.M.N., Rajapakse R.M.M.Y., Velauthamurti K. & Wijeratne S. (2010). Preparation and characterization of electronically conducting polypyrrole-montmorillonite nanocomposite and its potential application as a cathode material for oxygen reduction. *Electrochimica Acta* **55**(7): 2490–2497. DOI: https://doi.org/10.1016/j.electacta.2009.12.015

Senarathna K.G.C., Rajapakse R.M.G., Jayawardena P.S. & Kondo A. (2015). Extremely low-cost alternative for the oxygen reduction catalyst of fuel cell. *Advances in Automobile Engineering* **4**(1): 1–6. DOI: https://doi.org/10.4172/2167-7670.1000121

Senarathna K.G.C., Randiligama H.M.S.P. & Rajapakse R.M.G. (2016). Preparation, characterization and oxygen reduction catalytic activities of nanocomposites of Co(II)/montmorillonite containing polypyrrole, polyaniline or poly(ethylenedioxythiophene). *RSC Advances* **6**(114): 112853–112863. DOI: https://doi.org/10.1039/C6RA23100D

Singh P. & Buttry D. (2012). Comparison of oxygen reduction reaction at silver nanoparticles and polycrystalline silver electrodes in alkaline solution. *The Journal of Physical Chemistry C* **116**(19): 10656–10663. DOI: https://doi.org/10.1021/jp301676n

Sivanesan A., Witkowska E., Adamkiewicz W., Dziewit Ł., Kamińska A. & Waluk J. (2014). Nanostructured silver-gold bimetallic SERS substrates for selective identification of bacteria in human blood. *The Analyst* **139**: 1037–1043. DOI: https://doi.org/10.1039/c3an01924a

Sogandares F.M. & Fry E.S. (1997). Absorption spectrum (340-640 nm) of pure water. *Applied Optics* **36**(33): 8699–8709. DOI: https://doi.org/10.1364/AO.36.008699

Wang C., Markovic N.M., Stamenkovic V.R. (2012). Advanced platinum alloy electrocatalysts for the oxygen reduction reaction. *ACS Catalysis* **2**(5): 891–898. DOI: https://doi.org/10.1021/cs3000792

Wei Y., Li L., Yang X., Pan G., Yan G. & Yu X. (2010). One-step UV-induced synthesis of polypyrrole/ag nanocomposites at the water/ionic liquid interface. *Nanoscale Research Letters* **5**(2): 433–437. DOI: https://doi.org/10.1007/s11671-009-9501-9

Yao Z., Nie H., Yang Z., Zhou X., Liu Z. & Huang S. (2012). Catalyst-free synthesis of iodine-doped graphene via a facile thermal annealing process and its use for electrocatalytic oxygen reduction in an alkaline medium. *Chemical Communications* **48**(7): 1027. DOI: https://doi.org/10.1039/c2cc16192c